Classification: Biological Sciences, Neuroscience

Photolysis of a Caged Peptide Reveals Rapid Action of NSF Prior to Neurotransmitter Release

T. Kuner[1,2,*], Y. Li[1,2], K.R. Gee[3], L.F. Bonewald[4], and G.J. Augustine[1,2]

[1] Dept. Neurobiology, Duke Univ. Medical Center, Box 3209, Durham, NC 27710
[2] Marine Biological Laboratory, Woods Hole, MA 02543
[3] Invitrogen Corporation, Carlsbad, CA 92008
[4] University of Missouri at Kansas City, Kansas City, MO 64108-2784

* present address: Dept. of Anatomy and Cell Biology, University of Heidelberg, Im Neuenheimer Feld 307, 69120 Heidelberg, Germany.

Corresponding author: T. Kuner at the University of Heidelberg
kuner@uni-heidelberg. de
Phone: +49-6221-548678
Fax: +49-6221-544952.

Manuscript information: 23 text pages
7 figures
0 tables

Words and character count: Abstract : 113 words
Total number of characters: 46847
Number of characters text only : 33631
Number of characters figures: 13216

Abbreviations: CMNCBZ - ((5-carboxy-methoxy-2-nitrobenzyl)oxy)carbonyl
NSF - *N*-ethylmaleimide-sensitive factor
PSC – postsynaptic current
SNARE - soluble NSF attachment protein receptor
SV – synaptic vesicle

Data deposition:

Abstract

The time at which the *N*-ethylmaleimide-sensitive factor (NSF) acts during synaptic vesicle trafficking was identified by time-controlled perturbation of NSF function with a photo-activatable inhibitory peptide. Photolysis of this caged peptide in the squid giant presynaptic terminal caused an abrupt (0.2 s) slowing of the kinetics of the postsynaptic current (PSC) and a more gradual (2-3 s) reduction in PSC amplitude. Based on the rapid rate of these inhibitory effects relative to the speed of synaptic vesicle recycling, we conclude that NSF functions in reactions that immediately precede neurotransmitter release. Our results indicate the locus of SNARE protein recycling in presynaptic terminals and reveal a new target for rapid regulation of transmitter release.

Introduction

Neurotransmitter release relies on the precisely coordinated actions of many proteins that serve to recruit synaptic vesicles (SV) to active zones, prepare SVs for Ca^{2+}-dependent exocytosis, and recycle used components (1-5). At the core of these trafficking reactions lies the SNARE (soluble NSF attachment protein receptor) complex, which consists of proteins present in synaptic vesicles (v-SNAREs) and the plasma membrane (t-SNAREs) (6). It is thought that *trans*-SNARE complexes bridging the SV and plasma membranes bring these two membranes into close apposition and mediate membrane fusion (7, 8). Because SNARE complexes are highly stable, hydrolysis of ATP by the molecular chaperone NSF (9, 10) is required to disassemble used SNARE complexes and, thereby, recycle SNARE proteins in preparation for future rounds of exocytosis (11-13). Although it is generally agreed that this action of NSF is important for neurotransmitter release, it is not clear whether NSF works before or after vesicle fusion. This distinction is critical for understanding the dynamic control of synaptic transmission by NSF and for elucidating the life cycle of SNARE complexes during SV trafficking.

Two models have been proposed for the timing of NSF action during neurotransmitter release (Fig. 1). SNAREs could be disassembled just before fusion, meaning that NSF is active only when needed for a fusion reaction (Fig. 1A). This is consistent with observations that NSF is required prior to vesicle fusion in several experimental systems (14-20). Alternatively, NSF could dissociate SNARE complexes immediately after neurotransmitter release (Fig. 1B). Such a post-fusion action of NSF could provide an attractive mechanism for sorting of v- and t-SNAREs following fusion: in this case, newly separated v-SNAREs would be carried along as recycled SVs bud from the plasma membrane, while t-SNAREs would remain behind in the plasma membrane. Although experimental evidence supporting this conclusion is limited (21, 22),

the ability to explain SNARE sorting makes a post-fusion action of NSF part of most current models of SV trafficking (8, 23-26).

One way to distinguish between these two alternatives is to inactivate the function of NSF acutely in living presynaptic nerve terminals. A post-fusion block of NSF would slowly inhibit transmitter release, over the 45-90 seconds required for SV cycling (27), while a pre-fusion block would more rapidly inhibit release (Fig. 1C). We therefore designed and synthesized a light-sensitive (caged) inhibitor of NSF. Our strategy was based on incorporating a caging group onto a key amino acid of a peptide that blocks the αSNAP-stimulated ATPase activity of NSF *in vitro* (28-30). This peptide prevents the NSF-mediated disassembly of the SNARE complex (28) and inhibits neurotransmitter release when injected into presynaptic terminals (30, 31).

By using this caged peptide to perturb NSF function, we found that the amount of neurotransmitter release was inhibited with a latency ranging from 1.6 to 3.2 s. Furthermore, the kinetics of neurotransmitter release was decreased even more rapidly, with a latency of 0.2 s. These very rapid actions of the uncaged inhibitory peptide lead us to conclude that the physiologically relevant locus of NSF action in the synaptic vesicle cycle is immediately upstream of membrane fusion and release of neurotransmitter.

Results

Design of caged NSF3 peptide

Our caged NSF inhibitor was based on the NSF3 peptide (30) derived from the D1 domain of squid NSF (Fig. 2A,B). Structural data suggests that the amino acid residues constituting this peptide are located at the external surface of the D1 domain, in close proximity to the N domain (Fig. 2B, blue). A glycine residue within this segment of NSF (Fig. 2A, underlined) is critical for the actions of both NSF (32, 33) and the NSF3 peptide (30). We sought to disrupt the active conformation of the peptide by placing a caging group onto the side chain of an amino acid near this glycine. For this purpose, we used a ((5-carboxy-methoxy-2-nitrobenzyl)oxy)carbonyl (CMNCBZ) cage (Fig. 2C) that was attached to a surface-exposed lysine residue (Fig. 2A, red) two residues upstream of the critical glycine residue. Following UV illumination, photolysis of this cage proceeds in two steps (Fig. 2C). The first step takes less than 1 ms and causes most of the cage to dissociate from the peptide; the second step, a spontaneous decarboxylation, is half-complete within 4.5 ms (34). The photolyzed peptide may assume its active conformation after the first step, but after the subsequent decarboxylation step it should be identical to the non-caged NSF3 peptide. Therefore the peptide should be in an active conformation within a few ms or less after UV illumination.

Photolysis of caged peptide inhibits neurotransmitter release

To define when NSF is required in the SV cycle, the caged NSF3 peptide (cNSF3) was microinjected into the presynaptic terminal of the squid giant synapse at concentrations of 0.05-2.5 mM, while monitoring synaptic transmission via recordings of presynaptic and postsynaptic (PSPs) potentials. The CMNCBZ cage masked the inhibitory activity of the peptide, because in each of 66 experiments uncaging the peptide with a brief pulse of UV light inhibited synaptic transmission (Fig. 3A). The time course of this block was rapid, occurring within

a few seconds or less (Fig. 3B). Synaptic transmission decreased during cNSF3 injection, indicating that the cage did not completely neutralize peptide activity (Fig. 3C). However, the CMNCBZ cage caused a four-fold increase in the IC_{50} of caged NSF3 (0.35 ± 0.08 mM) compared to non-caged peptide (0.08 ± 0.01 mM), which gave us sufficient dynamic range to control NSF function.

Previous work has established the specificity of non-caged NSF3 peptide. Key arguments are that: (i) both NSF3 and another peptide from the external surface of the D1 domain have identical inhibitory effects both on ATPase activity and on synaptic transmission; and (ii) mutation of the glycine residue, which inhibits NSF function *in vivo* (32, 33), completely abolishes the ability of NSF3 to inhibit both ATPase activity and synaptic transmission (30). Mass spectroscopy reveals that exposure to UV light produces a peptide that is identical to non-caged NSF3 (unpublished data), so that the biochemical properties of NSF3 defined in previous work (30, 31) should fully apply to uncaged cNSF3. Nonetheless, to consider possible side-effects of uncaging cNSF3, we performed two control experiments. First, we uncaged a scrambled NSF3 peptide. This peptide had the same amino acid composition as cNSF3, including the presence of a CMNCBZ-caged lysine residue, but does not resemble NSF3. In a total of 11 experiments, photolysis of this control peptide produced no effect on synaptic transmission, even when illuminating the terminal with up to 750 mJ/mm^2 and at free cage concentrations as high as 0.9 mM (Fig. 3D). Photolysis of a second control compound, CMNCBZ-caged rhodamine, was similarly ineffective (n = 5; data not shown). These results indicate that inhibition of neurotransmitter release was caused directly by the liberated NSF3 peptide, rather than being caused by UV illumination or by production of free CMNCBZ cage or CO_2. Thus, caging a single lysine residue decreased the biological activity of the NSF3 peptide about 4-fold, allowing flash photolysis to very rapidly control the molecular machinery of neurotransmitter release.

The NSF3 peptide both decreases synaptic transmission and slows the kinetics of neurotransmitter release (30). To determine the relationship between these two actions, we examined how quickly each developed following cNSF3 photolysis. For this purpose, postsynaptic currents (PSCs) were recorded while photolyzing cNSF3. Figure 4A shows a series of simultaneous pre- and postsynaptic recordings during photolysis of cNSF3. PSCs were elicited every second, with the pre-flash PSC shown as a black trace. Following a pulse of UV light, which was applied at the same time as a presynaptic action potential, the next PSC was virtually unchanged in amplitude yet clearly had slower kinetics (Fig. 4A, largest red trace). Both PSC rise time and decay were slowed following peptide uncaging, as readily observed when comparing PSCs scaled to the same peak amplitude (Fig. 4B). While this change in PSC kinetics was virtually immediate, occurring in less than 1 second, the inhibition of PSC amplitude required several seconds for completion (Fig. 4C). Similar results were obtained in a total of 14 experiments. Hence, temporally precise activation of the caged peptide revealed distinct time courses for the two actions of NSF3: a fast effect on the kinetics of neurotransmitter release and a slower effect on the amount of neurotransmitter released.

Time course of the two responses to uncaged NSF3

We quantified the time course of the slow effect of NSF3 by fitting exponential functions to data such as those shown at the top of Fig. 4C. The time constant for inhibiting PSC amplitude was activity-dependent and ranged from 3.1 s at 0.2 Hz to 1.6 s at 5 Hz (Fig. 5A). This acceleration of the rate of inhibition at higher rates of stimulation is consistent with previous observations of the activity-dependence of this peptide (30) and full-length NSF (32, 33). Uncaged NSF3 also had some effect in the absence of activity: when stimulating at 0.2 Hz, the first PSC evoked 5 seconds after photolysis of the peptide was reduced by 75% (Fig. 5A). This may reflect a continuous activity of NSF (20) in the resting

presynaptic terminal. Thus, NSF regulates the amount of neurotransmitter release over a time scale of a few seconds or less.

Given the rapid effect of uncaged NSF3 upon release kinetics, a different procedure was needed to determine the time course of this effect. For this purpose, we uncaged cNSF3 at different intervals preceding an action potential (Fig. 5B, inset). At very brief time intervals, the amount of slowing of PSC kinetics was minimal, but the slowing effect was complete if the light flash occurred 1 s before the synapse was activated. The relationship between pre-flash interval (Δt) and degree of slowing of the PSC decay was described by an exponential function with a time constant of 0.22 s (Fig. 5B). This time constant represents an upper estimate of the time period when NSF3 affects release kinetics, because of possible delays associated with photolysis of the CMNCBZ cage and with binding of uncaged NSF3 peptide to its target. Therefore, NSF regulates the kinetics of release over a time scale of 0.22 s or faster.

Because the time scales of the inhibitory effects of uncaged NSF3 peptide are very rapid relative to the tens of seconds or longer required for vesicles to recycle via conventional (45 - 90 s (27)) or kiss-and-run (t ~ 20 s (35, 36)) mechanisms of endocytosis, our data argue that NSF is required before neurotransmitter release occurs rather than acting after membrane fusion (Fig. 1). However, the high rate of synaptic activity in the experiments shown in Figs. 5A and 5B may cause a redistribution of SNARE complexes to the plasma membrane; if NSF was required to dissociate these *cis*-SNARE complexes after fusion, then inhibiting such a post-fusion action of NSF might prevent transmitter release by accumulating SNARE complexes in the plasma membrane. To examine this possibility, the experiments were repeated at a minimal rate of synaptic activity (0.03 Hz). The rate of onset of the kinetic effect was very similar at this low rate of stimulation, with a time constant of approximately 0.5 s (Fig. 5C). This reveals that uncaged NSF3 peptide rapidly slows the kinetics of

release even under conditions where plasma membrane accumulation of SNARE complexes should be minimal, reinforcing the conclusion that NSF works before membrane fusion.

The temporally distinct effects of uncaged NSF3 on release magnitude and kinetics suggest that the peptide causes these two effects via separate mechanisms. Further support for this comes from analysis of the concentration-dependence of these two effects (Fig. 5D). The fast effect occurred at higher concentrations of NSF3 (IC_{50} of 0.28 ± 0.02 mM) than the slow effect (IC_{50} of 0.06 ± 0.01 mM). Thus, binding of NSF3 at two different sites may affect two separate NSF-dependent reactions: a higher affinity one that slowly affects the magnitude of transmitter release and a lower affinity one that rapidly affects the kinetics of release. Alternatively, NSF3 may bind at only one site, with the difference in affinity and functional effects reflecting different conformational states of the binding site (e.g. ATP- versus ADP-bound states of NSF (12, 37)).

NSF3 does not prevent membrane fission

To further address a possible post-fusion role for NSF, we asked whether photolysis of cNSF3 directly affects endocytic membrane retrieval. By taking advantage of the slower kinetics of endocytosis relative to exocytosis, we could temporally uncouple endocytosis from exocytosis by selectively uncaging cNSF3 after exocytosis was completed. Presynaptic membrane capacitance was directly measured at the nerve terminal in the unperturbed state (Fig. 6, upper panel) and immediately following cNSF3 photolysis (Fig. 6, red). After an initial increase in capacitance, due to exocytosis triggered by high-frequency stimulation (grey area), the capacitance decreased gradually to baseline. The decays could be described with exponential functions with time constants of 149 ± 29 s before and 131 ± 22 s after photolysis of cNSF. These values were not significantly different (N=5, p=0.15, t-test), indicating that the speed of

endocytosis is not affected by inhibiting NSF function. Thus, if NSF has any post-fusion role, this role does not affect the rate of membrane fission during endocytosis and is not rate-limiting for exocytosis.

Discussion

We have used a caged inhibitor peptide to provide novel information about the timing of NSF action in synaptic vesicle trafficking. Our studies provide much higher time resolution (milliseconds) than was possible in previous work, including studies of a *Drosophila* temperature-sensitive NSF mutation (22,33). Because of this high time resolution, we could determine for the first time that NSF participates in two rapid reactions with time constants of a few seconds or less. Both the fast (0.22 s) and slow (2-3 s) effects of the NSF3 peptide occur on a time scale much faster than synaptic vesicle endocytosis and recycling (27, 35, 36), we conclude that these effects represent pre-fusion actions of NSF (Fig. 7). Formally speaking, NSF could still have additional actions after vesicle fusion (22). While our capacitance measurements indicate that NSF action is not required for endocytic membrane retrieval, other post-fusion actions could be masked by the rapid onset of photolyzed peptide and therefore remain undetected. Nevertheless, our results indicate that a pre-fusion action of NSF must be responsible for the ability of this chaperone to regulate the magnitude and kinetics of transmitter release. This extends previous work, largely done in non-neuronal cells, suggesting that NSF participates in vesicle priming and resolves a long-standing question about when NSF functions in synaptic vesicle trafficking.

The slower, activity-dependent reaction occurring on a time scale of several seconds likely reflects the disassembly of *cis*-SNARE complexes upon docking of

SV at the active zone (steps 1-3 in Fig. 7). Inhibition of the αSNAP-stimulated ATPase activity of NSF by uncaged NSF3 peptide (30) would prevent NSF-dependent disassembly of *cis*-SNARE complexes (28) and thereby reduce the amount of uncomplexed SNARE proteins available after SVs are docked at the active zone. This would reduce the amount of neurotransmitter release, which requires formation of *trans*-SNARE complexes (3-5), and could account for the increase in docked SVs in terminals injected with NSF3 (30) as well as the accumulation of transport vesicles at acceptor membranes in the absence of NSF (38, 39). Thus, NSF appears to prime tethered SVs for release, as previously concluded for non-neuronal forms of membrane fusion and also suggested for neurotransmitter release (14-20). This can account for the activity-dependence of NSF3 action: synaptic transmission would not be inhibited immediately after uncaging cNSF3, because of the presence of primed SVs at the active zone. Only after the activity-dependent depletion or time-dependent depriming of these SVs (20, 40) would the requirement for NSF to prime SVs become evident. It therefore appears that NSF disassembles *cis*-SNARE complexes over a time scale of a few seconds under physiological conditions. Sorting of disassembled v- and t-SNARE proteins to their appropriate compartments would then occur by the binding to compartment-specific partners during or shortly after fusion (Fig. S2, arrow). Such a mechanism permits sorting of SNAREs while the membrane domains of SVs and the plasma membrane retain their identity. It can also account for experimental observations that SNARE complexes containing both v- and t-SNAREs exist in vesicle membranes (41-47) and that v-SNAREs can remain on the plasma membrane after endocytosis (48).

At first glance, this model could be challenged by biochemical measurements suggesting that both SVs and the plasma membrane contain an excess of free SNARE proteins (47, 49, 50), making the pre-fusion production of free SNARE proteins for *trans*-SNARE complex formation unnecessary. However,

biochemical studies consider mainly bulk compartments such as reserve pool vesicles or total plasma membrane, precluding extrapolation to the subset of SNARE proteins directly involved in exocytosis. Further, the presence of even a small number of *cis*-SNARE complexes at the fusion site might serve as a steric hindrance to membrane fusion, despite the presence of free SNARE proteins.

In addition to *cis*-SNARE complexes, NSF could act upon several other protein complexes. For example, αSNAP recruitment to a complex containing only syntaxin and SNAP-25 (51, 52) causes strong stimulation of NSF ATPase activity and complex disassembly (53). Tomosyn/t-SNARE complexes also can be disassembled by αSNAP-stimulation of NSF (54). These mechanisms could regulate the availability of a pool of plasma membrane t-SNARES for the formation of *trans*-SNARE complexes. NSF has been suggested to regulate the trapping of t-SNAREs into hotspots by dynamin (55). The ATPase activity of NSF could release t-SNARES from this trap just prior to *trans*-SNARE pairing and membrane fusion (55). In summary, photolysis of cNSF3 could cause abrupt freezing of *cis*-SNARE complexes, binary SNARE complexes, tomosyn-t-SNARE complexes and/or t-SNARE/dynamin complexes. Such effects, either separately or in concert, could account for the slower, activity-dependent component of the response to uncaged NSF3. Together, these mechanisms may constitute the contributions of NSF to ATP-dependent priming (42) of SVs.

The fast NSF-dependent reaction that affects release kinetics (steps 3-4 in Fig. 7) could result from a desynchronization of release events or a direct modulation of the fusion reaction by NSF, as has been suggested in other studies (56-58). The fast NSF3 effect is similar in time course to priming of the fusion machinery, which precedes release by 45-250 ms (59) and requires ATP hydrolysis (14, 60, 61). Although the rate of αSNAP-stimulated ATPase activity in the native environment of the nerve terminal is unknown, the ATPase activity of NSF *in vitro* (62) appears to be too slow to support a reaction that occurs within a time scale of 0.2 seconds. The fast effect could be related to an ATPase-independent

function of NSF (56), perhaps aiding proper folding and zippering up of SNARE complexes or optimizing the state of oligomerization of SNAREs (63).

In conclusion, or work indicates that NSF function is critical for highly dynamic reactions that occur immediately before synaptic vesicles fuse with the presynaptic plasma membrane to release neurotransmitter. In addition to answering a long-standing question about the timing of NSF action during synaptic vesicle trafficking, our results indicate a new potential locus for rapid regulation of neurotransmitter release by signals such as nitric oxide (28) or protein kinases (64-66). Our work also is the first to define the precise timing of any protein-protein interaction involved in synaptic vesicle exocytosis, hence providing a temporal benchmark for future studies of the timing of other exocytotic interactions.

Materials and Methods

Caged peptides

5-(carboxymethoxy)-2-nitrobenzyloxycarbonyl (CMNCBZ) caged lysine (67, 68) was synthesized as described in Supplementary Information. This peptide was used to synthesize the following peptides: Caged NSF3, TGKTLIAR[K]IGKMLNATEPK (squid sequence), caged scrambled NSF3 = GNIELATKT[K]ARIKLTMPKG. Details of peptide synthesis are provided in Supplementary Information.

Electrophysiology

The stellate ganglion was dissected from *Loligo pealei* and recordings of synaptic transmission were done as described previously (69, 70). Caged peptide was microinjected into the giant presynaptic terminal and a shuttered argon ion laser (Coherent Inc., Santa Clara, CA) was used for peptide photolysis.

More details are described in Supplementary Information.

Acknowledgements

We thank H. Tokumaru for many discussions and helping with biochemical experiments, J. Rizo for suggesting - and F. Filipp and M. Sattler for performing - NMR interaction studies of the NSF3 peptide with NSF domains, and Phyllis Hanson for discussions.

T.K. was supported by a Grass Fellowship in Neuroscience, an HFSP long-term fellowship and the Feodor-Lynen Program of the Alexander von Humboldt Foundation. Y.L. received a American Heart Association predoctoral fellowship. The research also was supported by NIH NS-21624.

Author contributions

T.K. designed and carried out experiments and wrote the manuscript. Y.L. did experiments. K.R.G. synthesized the caged lysine. L.F.B. made the caged peptide. G.J.A. designed experiments and wrote the manuscript.

Figure Legends

Figure 1: Pre or post fusion function of NSF

A. Model depicting NSF acting upstream of neurotransmitter release. NSF (yellow), αSNAP (green), v-SNARE (blue), t-SNAREs (orange).

B. Model showing a post-fusion role of NSF.

C. Because the synaptic vesicle (SV) cycle requires 45-90 seconds *(left)*, a pre-fusion block of NSF action would occur much more quickly *(center)*, while a post-fusion block would require all or most of the 45-90 seconds *(right)*.

Figure 2: Design of the caged NSF3 peptide (cNSF3)

A. Sequence of the squid NSF3 peptide. Underlined residue is G309, the Comatose locus (corresponds to G274 in NSF-1 of *Drosophila*) and the caged lysine residue K307 is in red and is marked with an asterisk.

B. Schematic representation of NSF with structural elements contributing to the lateral surfaces of the N and D1 domains. *Upper* - N, D1 and D2 denote the three domains of a NSF monomer, the schematic side-view shows only three subunits of the hexamer. *Lower* – Predicted structure of the N and D1 domains of NSF, based on coordinates taken from the NSF homologue P97(71). The 2.5 nm thick slab shows: N-domain in orange, D1-domain in yellow, the NSF3 peptide in blue, and the caged lysine residue in red. Other active NSF peptides (30) are indicated in green (NSF1) and purple (NSF2).

C. Photochemistry of CMNCBZ-caged lysine. Absorption of a photon of UV light rapidly removes most of the cage, while a slower spontaneous decarboxylation removes the rest and generates free CO_2 (34).

Figure 3: Photolysis of cNSF in the presynaptic terminal

A. Inhibition of synaptic transmission after uncaging microinjected cNSF3 (0.75 mM) in the giant terminal of the squid. Action potentials were elicited every 1 s.

Simultaneous presynaptic (V_{pre}) and postsynaptic (V_{post}) voltage recordings immediately before (black) and after (red) uncaging (stimulation artefact blanked).

B. Rapid time course of inhibitory effects of uncaged NSF3. The slope of the PSP was determined from fits to the initial rise of the PSP and plotted as a function of time. UV light was applied for 50 ms (arrow, ~ 150 mJ/mm^2). Terminal injected with 0.75 mM cNSF3.

C. Concentration-dependent inhibition of synaptic transmission by caged NSF3 peptide (black closed circles, n=14) and uncaged peptide (red open circles, n=14). See Supplementary Methods for further details.

D. Lack of effect of photolysis of caged scrambled NSF3 peptide (0.64 mM). UV light (750 mJ/mm^2) was applied three times at the point indicated by the arrow.

Figure 4: Differential onset of amplitude and kinetic effect

A. Simultaneous pre - and postsynaptic recordings before (black line) and after (red line) photolysis of caged NSF3 peptide. Synapse was stimulated at 1 Hz.

B. Scaled PSCs, from the experiment shown in A, before (black) and after (red) uncaging of NSF3.

C. Onset of changes in PSC amplitude *(top)*, PSC rise time (20-80%; *center*) and PSC decay time constant *(lower)*. UV light (150 mJ/mm^2) was applied at the 10 s time point (gray bar).

Figure 5: Activity-dependency and onset of fast effect

A. Time course of the slow effect of uncaged NSF3 on PSC amplitude. The fractional reduction of PSC amplitude is plotted as a function of time after peptide photolysis. Continuous curves are exponential functions with time constants of 1.6 s (5 Hz) and 3.1 s (0.2 Hz). Data points reflect 7 and 10 independent experiments, respectively.

B. Time course of the rapid effect of uncaged NSF3 on PSC kinetics. The

fractional slowing of PSC decay time constant is plotted as a function of the time interval (Δt) between the UV light flash (UV) and the presynaptic stimulus (AP_{pre}). The experimental protocol is illustrated in the inset. Data from 8 independent experiments using two stimulus frequencies (0.2 Hz; circles and 1 Hz; triangles) were pooled (squares) because the two data sets did not differ. The continuous curve is an exponential function with a time constant of 0.22 s.
C. Time course of the rapid inhibition of PSC kinetics by uncaged NSF3 under conditions of minimal synaptic activity (0.03 Hz). The continuous curve is an exponential function with a time constant of 0.5 s. Each point is from 2-5 experiments.
D. Concentration-dependent inhibition of PSC amplitude (open circles, IC50 = 0.28 ± 0.02 mM) and decay kinetics (closed circles, IC50 = 0.06 ± 0.01 mM) by uncaged NSF3). Each point is from 3-9 experiments.

Figure 6: Endocytosis unaffected by cNSF photolysis

Time course of endocytosis before (grey) and after (red) photolysis of cNSF3. Relative Cm change shown as a range (mean ± SEM, grey zone and space between red lines) Five independent experiments. High frequency stimulation (grey bar), photolysis immediately thereafter.

Figure 7: Model of NSF function and life-cycle of SNARE proteins

Model for the dual actions of NSF in transmitter release. A complete cycle of SV trafficking requires 45-90 seconds (27). After vesicle docking (1-2 transition), the slow action of NSF primes synaptic vesicles over a time scale of seconds. Readily releasable vesicles (3; highlighted red) can then fuse in a calcium-dependent reaction that is influenced by NSF acting within a time window of less than 0.5 seconds. Following membrane fusion, vesicles bud off from the plasma membrane (5-6 transition) and are then recycled (6-1 transition).

References

1. Augustine, G. J., Burns, M. E., DeBello, W. M., Hilfiker, S., Morgan, J. R., Schweizer, F. E., Tokumaru, H. & Umayahara, K. (1999) *J Physiol* 520 Pt 1, 33-41.

2. Rettig, J. & Neher, E. (2002) *Science* 298, 781-785.

3. Jahn, R. & Sudhof, T. C. (1999) *Annu Rev Biochem* 68, 863-911.

4. Sudhof, T. C. (1995) *Nature* 375, 645-53.

5. Rothman, J. E. (1994) in *Nature*, Vol. 372, pp. 55-63.

6. Sollner, T., Whiteheart, S. W., Brunner, M., Erdjument, B. H., Geromanos, S., Tempst, P. & Rothman, J. E. (1993) *Nature* 362, 318-24.

7. Weber, T., Zemelman, B. V., McNew, J. A., Westermann, B., Gmachl, M., Parlati, F., Sollner, T. H. & Rothman, J. E. (1998) *Cell* 92, 759-72.

8. Jahn, R., Lang, T. & Sudhof, T. C. (2003) *Cell* 112, 519-533.

9. Block, M. R., Glick, B. S., Wilcox, C. A., Wieland, F. T. & Rothman, J. E. (1988) *Proc Natl Acad Sci U S A* 85, 7852-6.

10. Wilson, D. W., Wilcox, C. A., Flynn, G. C., Chen, E., Kuang, W. J., Henzel, W. J., Block, M. R., Ullrich, A. & Rothman, J. E. (1989) *Nature* 339, 355-9.

11. Sollner, T., Bennett, M. K., Whiteheart, S. W., Scheller, R. H. & Rothman, J. E. (1993) *Cell* 75, 409-18.

12. Hanson, P. I., Roth, R., Morisaki, H., Jahn, R. & Heuser, J. E. (1997) *Cell* 90, 523-35.

13. Zinsmaier, K. E. & Bronk, P. (2001) *Biochem Pharmacol.* 62, 1-11.

14. Banerjee, A., Barry, V. A., DasGupta, B. R. & Martin, T. (1996) *J Biol Chem* 271, 20223-6.

15. Burgoyne, R. D. & Williams, G. (1997) *Febs Lett* 414, 349-52.

16. Colombo, M. I., Taddese, M., Whiteheart, S. W. & Stahl, P. D. (1996) *J Biol Chem* 271, 18810-6.

17. Mayer, A., Wickner, W. & Haas, A. (1996) *Cell* 85, 83-94.

18. Nichols, B. J., Ungermann, C., Pelham, H. R., Wickner, W. T. & Haas, A. (1997) *Nature* 387, 199-202.

19. Tolar, L. A. & Pallanck, L. (1998) *J Neurosci* 18, 10250-6.

20. Xu, T., Ashery, U., Burgoyne, R. D. & Neher, E. (1999) *Embo J* 18, 3293-3304.

21. Grote, E., Carr, C. M. & Novick, P. J. (2000) *J Cell Biol.* 151, 439-452.

22. Littleton, J. T., Barnard, R. J., Titus, S. A., Slind, J., Chapman, E. R. & Ganetzky, B. (2001) *Proc Natl Acad Sci U S A* 98, 12233-8.

23. Chen, Y. A. & Scheller, R. H. (2001) *Nat Rev Mol Cell Biol* 2, 98-106.

24. Li, L. & Chin, L.-S. (2003) *Cell. Mol. Life Sci,* 60, 942-960.

25. Richmond, J. E. & Broadie, K. S. (2002) *Curr Opinion Neurobiol.* 12, 499-507.

26. Rizo, J. & Südhof, T. C. (2002) *Nat Rev Neurosci.* 3, 641-653.

27. Betz, W. J. & Wu, L. G. (1995) *Current Biology* 5, 1098-1101.

28. Matsushita, K., Morrell, C. N., Cambien, B., Yang, S. X., Yamakuchi, M., Bao, C., Hara, M. R., Quick, R. A., Cao, W., O'Rourke, B., Lowenstein, J. M., Pevsner, J., Wagner, D. D. & Lowenstein, C. J. (2003) *Cell* 115, 139-50.

29. Polgar, J. & Reed, G. L. (1999) *Blood* 94, 1313-8.

30. Schweizer, F. E., Dresbach, T., DeBello, W. M., O'Connor, V., Augustine, G. J. & Betz, H. (1998) *Science* 279, 1203-6.

31. Parnas, I., Rashkovan, G., O'Connor, V., El-Far, O., Betz, H. & Parnas, H. (2006) *J Neurophysiol* 96, 1053-60.

32. Kawasaki, F., Mattiuz, A. M. & Ordway, R. W. (1998) *J Neurosci* 18, 10241-9.

33. Littleton, J. T., Chapman, E. R., Kreber, R., Garment, M. B., Carlson, S. D. & Ganetzky, B. (1998) *Neuron* 21, 401-13.

34. Papageorgiou, G. & Corrie, J. E. T. (1997) *Tetrahedron* 53, 3917-3932.

35. Aravanis, A. M., Pyle, J. T. & Tsien, R. W. (2003) *Nature* 423, 643-647.

36. Gandhi, S. P. & Stevens, C. F. (2003) *Nature* 423, 607-613.

37. Brunger, A. T. & DeLaBarre, B. (2003) *FEBS Lett* 555, 126-33.

38. Malhotra, V., Orci, L., Glick, B. S., Block, M. R. & Rothman, J. E. (1988) *Cell* 54, 221-7.

39. Orci, L., Malhotra, V., Amherdt, M., Serafini, T. & Rothman, J. E. (1989) *Cell* 56, 357-68.

40. Murthy, V. N. & Stevens, C. F. (1999) *Nat Neurosci* 2, 503-7.

41. Hong, R. M., Mori, H., Fukui, T., Moriyama, Y., Futai, M., Yamamoto, A., Tashiro, Y. & Tagaya, M. (1994) *FEBS Lett* 350, 253-7.

42. Klenchin, V. A. & Martin, T. F. J. (2000) *Biochimie* 82, 399-407.

43. Otto, H., Hanson, P. I. & Jahn, R. (1997) *Proc Natl Acad Sci U S A* 94, 6197-201.

44. Steel, G. J., Tagaya, M. & Woodman, P. G. (1996) *Embo J* 15, 745-52.

45. Taubenblatt, P., Dedieu, J. C., Gulik-Krzywicki, T. & Morel, N. (1999) *J Cell Sci* 112, 3359-3367.

46. Ungermann, C., Sato, K. & Wickner, W. (1998) *Nature* 396, 543-8.

47. Walch-Solimena, C., Blasi, J., Edelmann, L., Chapman, E. R., von Mollard, G. F. & Jahn, R. (1995) *J Cell Biol* 128, 637-45.

48. Fernandez-Alfonso, T., Kwan, R. & Ryan, T. A. (2006) *Neuron* 51, 179-86.

49. Lang, T., Margittai, M., Holzler, H. & Jahn, R. (2002) *J Cell Biol* 158, 751-60.

50. Takamori, S., Holt, M., Stenius, K., Lemke, E. A., Gronborg, M., Riedel, D., Urlaub, H., Schenck, S., Brugger, B., Ringler, P., Muller, S. A., Rammner,

B., Grater, F., Hub, J. S., De Groot, B. L., Mieskes, G., Moriyama, Y., Klingauf, J., Grubmuller, H., Heuser, J., Wieland, F. & Jahn, R. (2006) *Cell* 127, 831-46.

51. Fasshauer, D., Otto, H., Eliason, W. K., Jahn, R. & Brunger, A. T. (1997) *J Biol Chem* 272, 28036-41.

52. An, S. J. & Almers, W. (2004) *Science* 306, 1042-6.

53. Matveeva, E. & Whiteheart, S. W. (1998) *FEBS Lett* 435, 211-4.

54. Hatsuzawa, K., Lang, T., Fasshauer, D., Bruns, D. & Jahn, R. (2003) *J Biol Chem* 278, 31159-66.

55. Peters, C., Baars, T. L., Buhler, S. & Mayer, A. (2004) *Cell* 119, 667-78.

56. Müller, J. M., Rabouille, C., Newman, R., Shorter, J., Freemont, P., Schiavo, G., Warren, G. & Shima, D. T. (1999) *Nat Cell Biolog* 1, 335-340.

57. Otter-Nilsson, M., Hendriks, R., Pecheur-Huet, E. I., Hoekstra, D. & Nilsson, T. (1999) *Embo J* 18, 2074-83.

58. Muller, O., Bayer, M. J., Peters, C., Andersen, J. S., Mann, M. & Mayer, A. (2002) *Embo J* 21, 259-69.

59. Zenisek, D., Steyer, J. A. & Almers, W. (2000) *Nature* 406, 849-54.

60. Holz, R. W., Bittner, M. A., Peppers, S. C., Senter, R. A. & Eberhard, D. A. (1989) *J Biol Chem* 264, 5412-9.

61. Parsons, T. D., Coorssen, J. R., Horstmann, H. & Almers, W. (1995) *Neuron* 15, 1085-96.

62. Tagaya, M., Wilson, D. W., Brunner, M., Arango, N. & Rothman, J. E. (1993) *J Biol Chem* 268, 2662-6.

63. Tokumaru, H., Umayahara, K., Pellegrini, L. L., Ishizuka, T., Saisu, H., Betz, H., Augustine, G. J. & Abe, T. (2001) *Cell* 104, 421-432.

64. Liu, Y., Cheng, K., Gong, K., Fu, A. K. & Ip, N. Y. (2006) *J Biol Chem* 281, 9852-8.

65. Matveeva, E. A., Whiteheart, S. W., Vanaman, T. C. & Slevin, J. T. (2001) *J Biol Chem* 276, 12174-81.

66. Huynh, H., Bottini, N., Williams, S., Cherepanov, V., Musumeci, L., Saito, K., Bruckner, S., Vachon, E., Wang, X., Kruger, J., Chow, C. W., Pellecchia, M., Monosov, E., Greer, P. A., Trimble, W., Downey, G. P. & Mustelin, T. (2004) *Nat Cell Biol* 6, 831-9.

67. Mitchison, T. J., Sawin, K. E., Theriot, J. A., Gee, K. & Mallavarapu, A. (1998) *Methods Enzymol* 291, 63-78.

68. Gee, K. R., Weinberg, E. S. & Kozlowski, D. J. (2001) *Bioorg Med Chem Lett* 11, 2181-3.

69. Augustine, G. J. & Eckert, R. (1984) *J Physiol (Lond)* 346, 257-71.

70. Augustine, G. J., Charlton, M. P. & Smith, S. J. (1985) *J Physiol (Lond)* 367, 143-62.

71. Zhang, X., Shaw, A., Bates, P., Newman, R., Gowen, B., Orlova, E., Gorman, M., Kondo, H., Dokurno, P., Lally, J., Leonard, G., Meyer, H., van Heel, M. & Freemont, P. (2000) *Mol Cell* 6, 1473-84.

Kuner et al., Figure 1

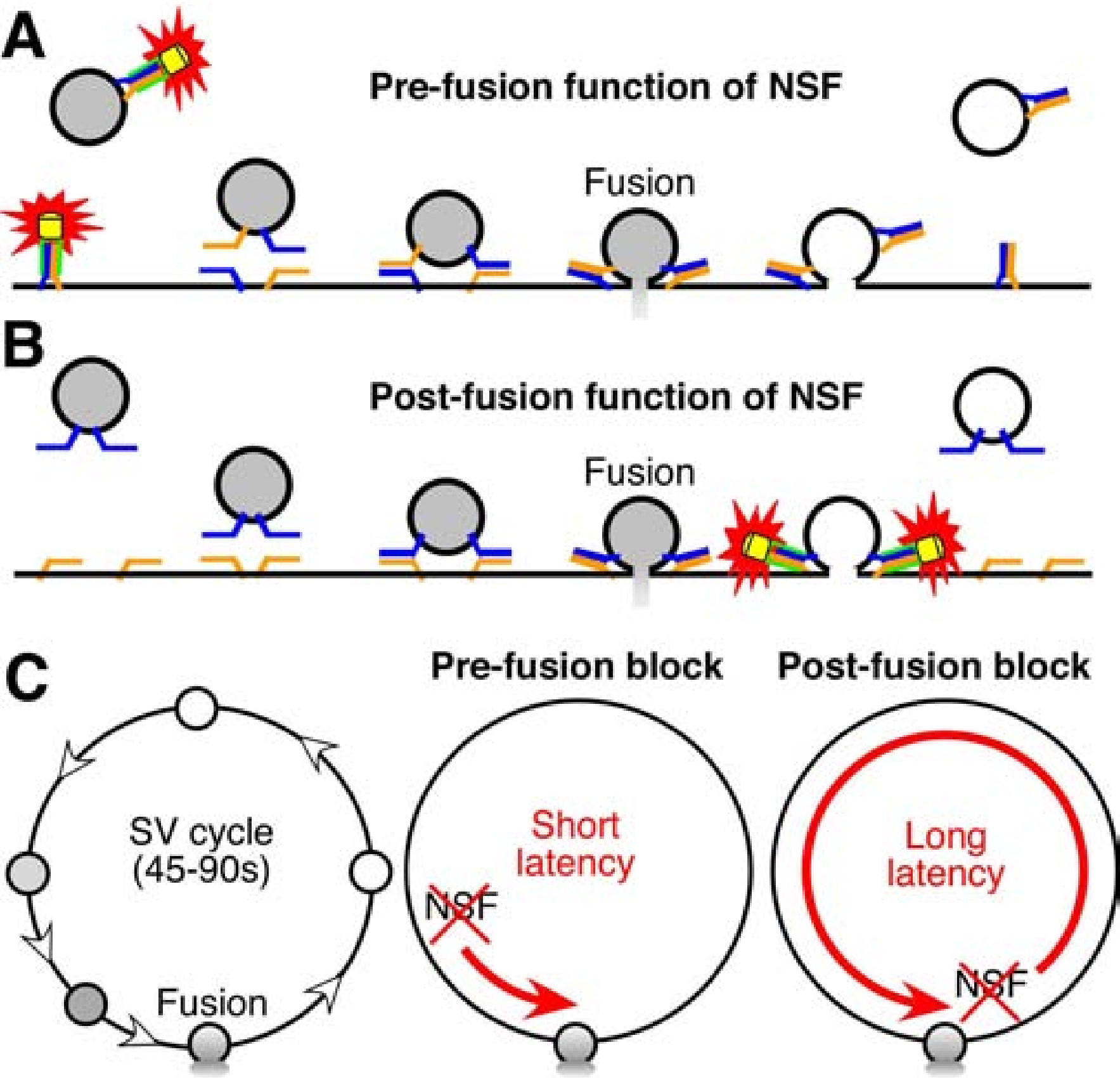

Kuner et al., Figure 2

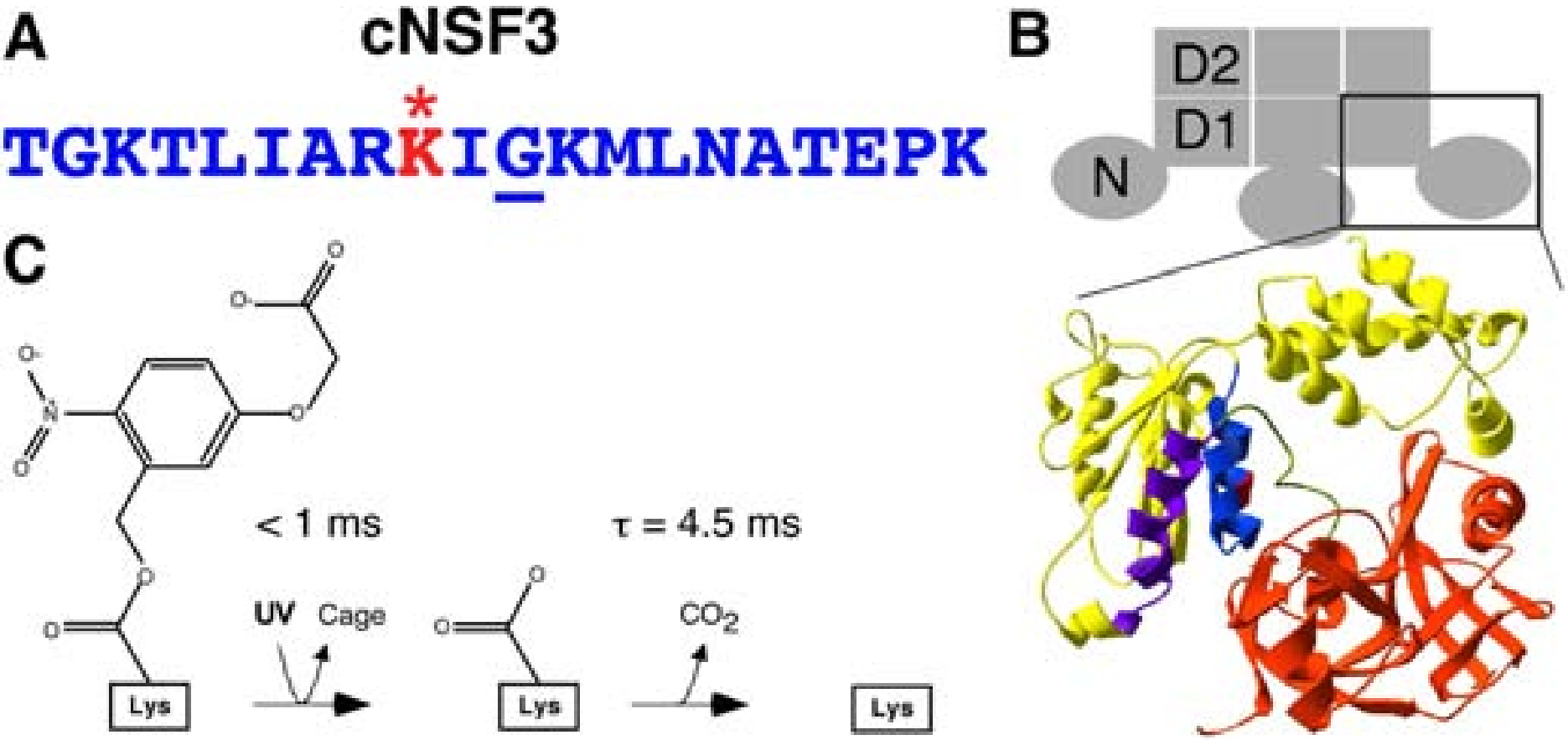

Kuner et al., Figure 3

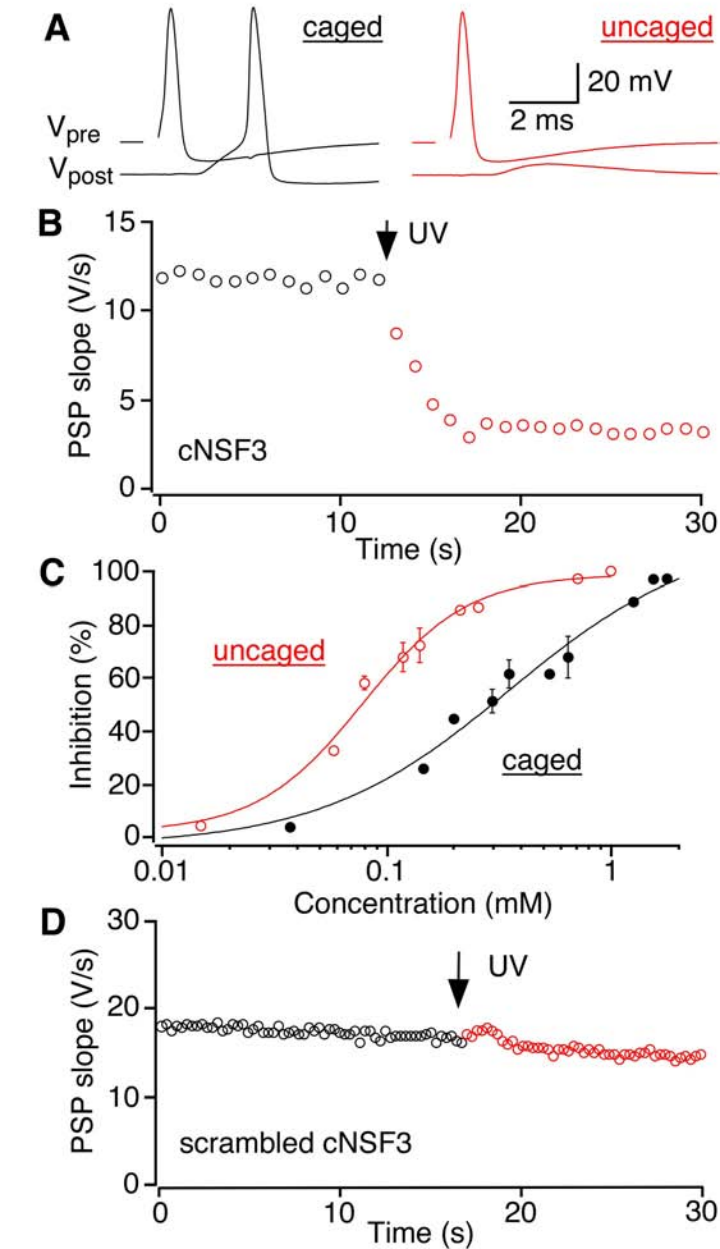

Kuner et al., Figure 4

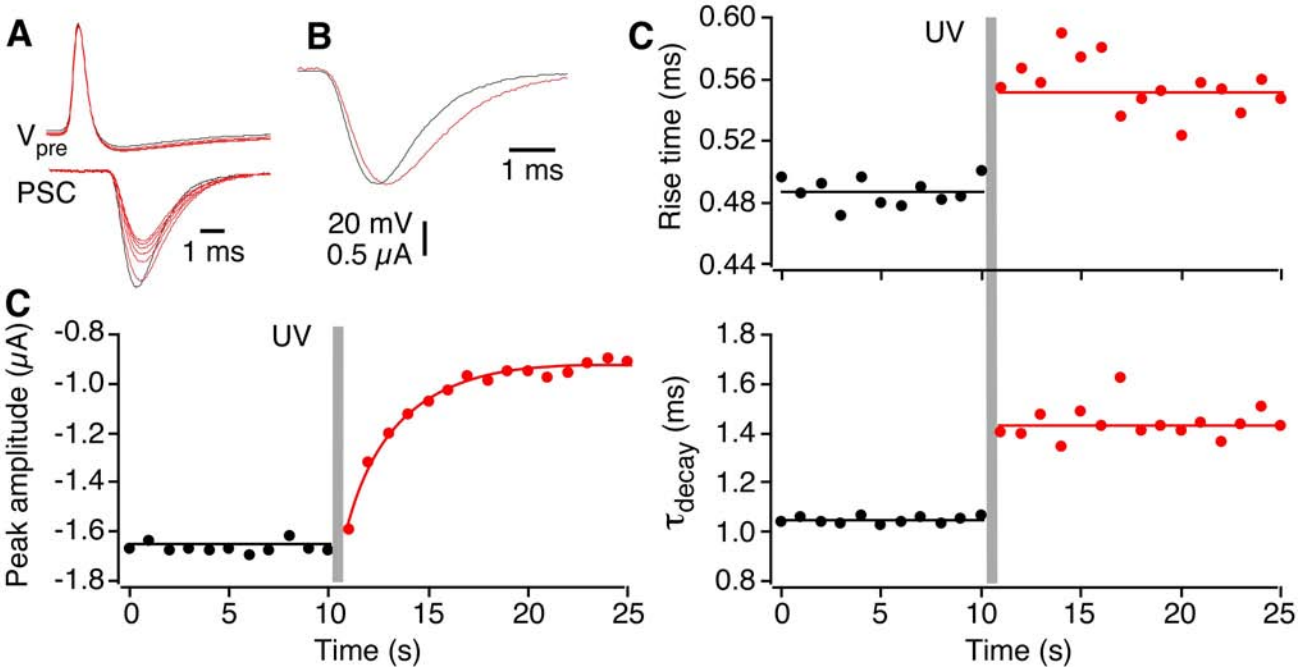

Kuner et al., Figure 5

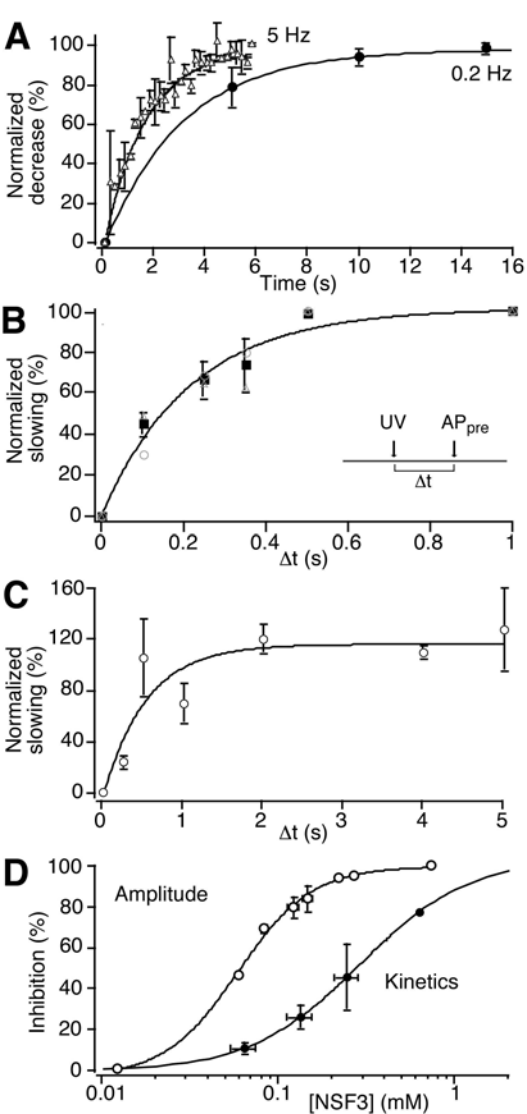

Kuner et al., Figure 7

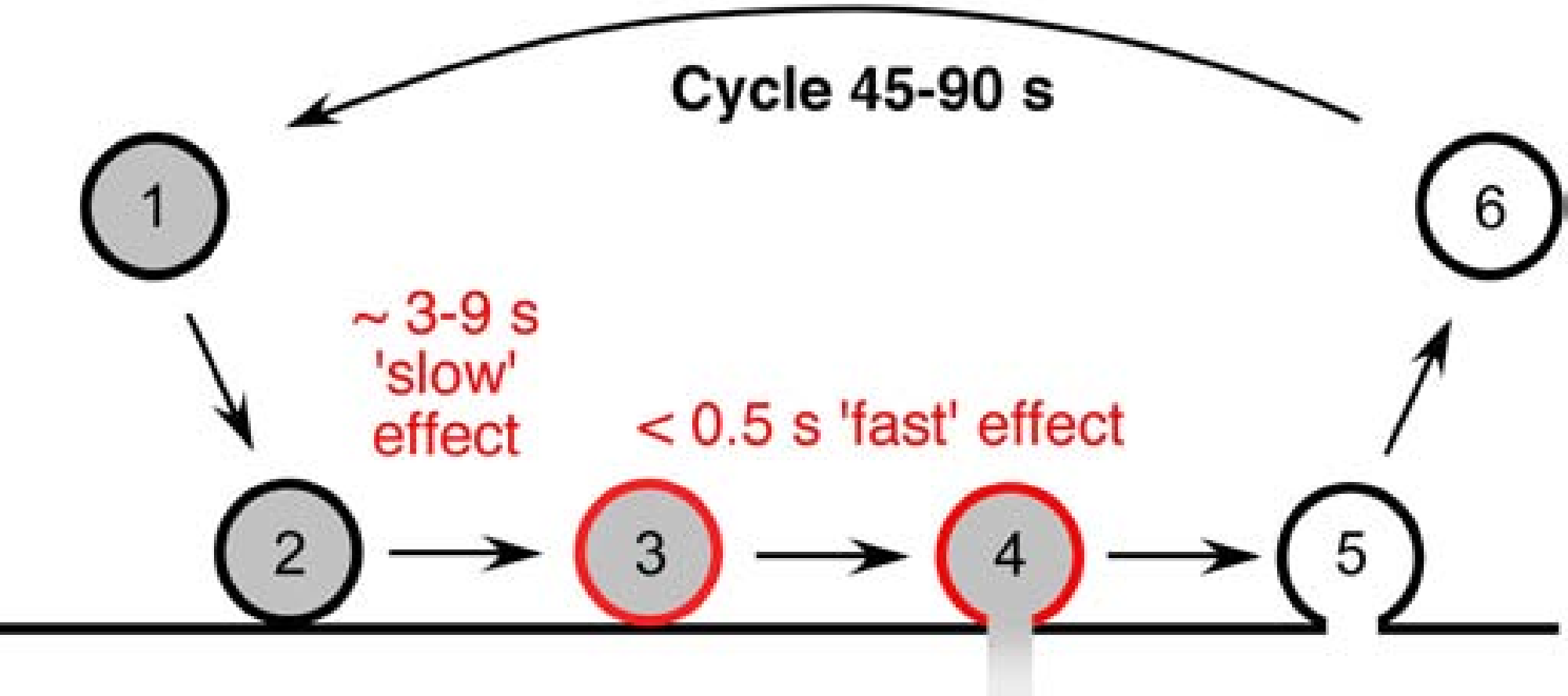

Supplementary Information

Materials and Methods

Chemical synthesis of caged lysine.

The 5-(carboxymethoxy)-2-nitrobenzyloxycarbonyl (CMNCBZ) caging group has been used successfully to cage the amino groups of fluorescent probes (1, 2). UV photolysis rapidly liberates a carbamic acid, which spontaneously decarboxylates to give the free amine. In the current experiments, the anionic carboxylate of the caging group functions to disguise the normal positive charge of the lysine residue side chain amino group to which it is attached, thus reducing the likelihood of it being recognized by the binding partner of NSF3. Before peptide synthesis, the caging group carboxylate was protected as an acid labile t-butyl ester. This strategy allows for normal FMOC-based solid phase peptide synthesis after incorporation of the caged lysine residue, but the caging group t-butyl ester is cleaved to a carboxylate upon acid-mediated cleavage of the final peptide from the synthesis resin.

e-(*t*-Bu-CMNCBZ)-a-FMOC-(L)-lysine. a-FMOC-(L)-lysine (5.88 g, 16 mmol) is added to a solution of the chloroformate of 5-(*t*-butoxycarbonylmethoxy)-2-nitrobenzyl alcohol (16 mmol) in 60 ml anhydrous dichloromethane, followed by diisopropylethylamine (32 mmol). The resulting mixture is stirred for 6h, then concentrated in vacuo. The residue is purified by flash chromatography using chloroform/methanol/acetic acid as eluant to afford e-(*t*-Bu-CMNCBZ)-a-FMOC-(L)-lysine as 3.88 g (36%) of a pale brown powder: ^{1}H NMR (CD_2Cl_2) d 8.15 (d, 1H), 7.71 (d, 2H), 7.61 (m, 2H), 7.40 (t, 2H), 7.29 (t, 2H), 7.08 (t, 1H), 5.33 (s, 2H), 4.82 (s, 2H), 4.34 (d, 2H), 4.23 (t, 1H), 3.17 (br d, 3H), 1.9 (m, 2H), 1.77 (m, 2H), 1.53 (m, 2H), 1.44 (s, 9H); m/z 678 (677 calculated for $C_{35}H_{39}N_3O_{11}$).

Caged peptides

The following peptides were synthesized: Caged NSF3,

TGKTLIAR[K]IGKMLNATEPK (squid sequence), caged scrambled NSF3 = GNIELATKT[K]ARIKLTMPKG. Peptides were synthesized on an Advanced Chemtech 396 MBS synthesizer using standard FMOC chemistry. All procedures were performed under reduced light conditions to prevent photolysis of the caged amino acids. FMOC-Rink amide MBHA resin was used to yield an amide at the carboxy terminus. The caged amino acids were synthesized as described above and non-caged amino acids were from Anaspec (San Jose, Ca). NMP was used for swelling the resin, Pip for deprotection and the amino acids were incorporated using HOBt/HBTU/DIEA activation, two couplings each. The caged amino acids were coupled only once overnight. The well plate was removed from the synthesizer, reagents added, covered in aluminum foil and placed onto the shaker (Ocelot). The next day the plate was put back onto the synthesizer, the fluids drained, and synthesis continued as normal. Most peptides were acetylated by the same coupling methods as above using 30% acetic anhydride in DMF. The peptides were cleaved while mixing in 94.5% TFA, 2.5% Water, 2% EDT, and 1% TIS at room temperature for 2 hours. The peptides were then precipitated with ethyl ether, placed at -80℃ for 2 hours, centrifuged for 30 minutes at 2000 rpm, decanted, and the pellet resuspended in sufficient formic acid to dissolve the pellet, followed by addition of 0.1% TFA/Water to equilibrate for application to HPLC. The peptides were purified on a Gilson HPLC using C18 reverse phase (Phenomenex column, 250 x 21.20mm, 10 micron, 300 Å); buffer A, 0.1% TFA/Water; buffer B, 0.1% TFA in acetonitrile. The fractions containing the correct peptide according to mass calculation were identified using MALDI (Perseptive Biosystems Voyager DE), then frozen, lyophilized, and stored at –22° C wrapped in aluminum foil.

Electrophysiology

The stellate ganglion was dissected from *Loligo pealei* supplied by the Marine Resources Center of the Marine Biological Laboratory. Simultaneous pre- and postsynaptic intracellular recordings from the giant synapse were carried out

with sharp electrodes positioned in the terminal and postsynaptic axon (3). Action potentials were stimulated with a third electrode in the presynaptic axon every 0.2 to 30s. The slope of the postsynaptic potential (PSP) in current-clamp recordings was taken as a measure of neurotransmitter release. To determine changes in the kinetics of release, the postsynaptic axon was voltage-clamped with a 2-microelectrode voltage clamp (Axoclamp-2A; Axon Instruments). Postsynaptic currents were filtered at 5 kHz and digitized at 33 kHz. The stellate ganglion was superfused at 14-15˚C with squid saline containing (in mM): 466 NaCl, 54 $MgCl_2$, 11 $CaCl_2$, 10 KCl, 3 $NaHCO_3$, and 10 HEPES, pH 7.2. Recording pipettes were filled with 3 M KCl or 7 M CsCl. Signals were digitized with a TL1 board and recorded with a custom-made software written in Axobasic by F. Schweizer (UCLA). Off-line analysis of kinetic parameters was done with an automized procedure written in Igor (WaveMetrics, Lake Oswego, OR). All numbers are given as mean ± SEM unless noted otherwise.

Peptide injection and photolysis

Lyophyllized peptide was dissolved in deionized water in the presence of 10% dimethylsulfoxide (DMSO) to facilitate solubility. The concentration of the peptide solution was 10 to 20 mM as determined spectrophotometrically ($l_{max,\ CMNCBZ}$ = 305 nm, e = 9200 $M^{-1}cm^{-1}$). Rhodamine dextran (10 µM, 10 kDa dextran, Molecular Probes) was added to the solution to monitor loading of the terminal and estimation of the free peptide concentration in the terminal. The injection solution was supplemented with 10 mM KCl to facilitate voltage recordings. Test injections of a 10% DMSO solution containing Rhodamine dextran did not affect neurotransmitter release (5 ± 7 % change in slope, n=4), presumably because DMSO diffused away as it was injected. Only terminals with damage-free recordings, as judged from lack of changes in neurotransmitter release following microelectrode impalements, were used. When testing caged scrambled NSF3 peptide, successful illumination was

confirmed by photolysing caged fluorescein dextran that was coinjected into the terminal (3 μM).

A constant wave argon ion laser (Coherent Inc., Santa Clara, CA) was used to generate UV light in the range of 342 to 354 nm with a total output power of about 2 W. The laser beam was directed into the specimen from below the microscope stage by using highly reflective mirrors (Newport Corporation, Irvine, CA). A uniform beam profile of about 1.2 mm diameter was produced in the focal plane of the specimen; this light spot covers the entire presynaptic terminal. A mechanical shutter (Vincent Associates, Rochester, NY) was used to control the amount of laser light (20 to 100 mJ). 50 mJ of UV light photolyzed ~40% of the cage, as determined with caged fluorescent dyes.

The dose-response curves shown in Fig. 3C were determined as follows. The curve for cNSF3, reflecting the residual activity of the caged NSF3 peptide, was established from the extent of inhibition caused by different concentrations of cNSF3 injected into the terminal. To generate the curve for uncaged NSF3 peptide, we first calculated its concentration by multiplying the cNSF3 concentration with the known uncaging efficiency. The observed degree of inhibition after photolysis reflected the combined presence of uncaged NSF3 and remaining cNSF3. The inhibition produced by uncaged NSF3 alone was derived by extrapolating the inhibitory effect of the remaining cNSF3 concentration from the cNSF3 curve and subtracting this value from the total inhibition.

Capacitance recordings

For presynaptic capacitance measurement, two microelectrodes were inserted into the presynaptic terminal to control presynaptic membrane potential under voltage clamp, similar as previously described(4). Membrane capacitance (Cm) was monitored in the two-electrode voltage-clamp configuration similar as previously reported(5). Briefly, Cm was determined from the current response to a triangular, symmetrical voltage command repetitively applied at up to 60

Hz. The hyper and depolarizing ramps (±25 mV in 4~10 ms) elicited membrane currents that were the sum of resistive and capacitive components. The capacitive current was determined by subtracting the down-ramp current integral from the up-ramp current integral. Then, dividing the capacitive current by the stimulus voltage yielded Cm.

Supplementary Discussion

Specificity of NSF3 peptides

The specificity of NSF peptides has been demonstrated by several studies using different paradigms (references 28-31). The arguments that the NSF peptides exert their effects specifically by interfering with NSF are as follows:

1) Two peptides derived from the D1 domain of NSF (NSF2 and NSF3) exert similar effect on the amplitude and kinetics of synaptic transmission, while three other peptides derived from the same domain do not show any effect at all. The segments of the domain from which the peptides were derived are spatially clustered at a location close to the ATP binding site, whereas the ineffective peptides were derived from regions which are exposed to the inside of the NSF multimer (Kuner, T., Tokumaru, H. & Augustine, G. J. (2002) in Peptide-lipid interactions, eds. Simon, S. A. & McIntosh, T. J. (Academic Press, San Diego), Vol. 52, pp. 552-570.). This seems to be very strong evidence for the specificity of peptide action, because there is very little chance that two peptides with completely different primary sequences would exert the same physiological effects.

2. It has been demonstrated that NSF2 and NSF3 peptides selectively interfere with ATPase function in a biochemical assay containing only aSNAP and NSF proteins (refs. 29, 30). The inhibition of ATPase function occurred at peptide concentrations similar to those used in the nerve terminal (ref. 30). It also has been demonstrated that the NSF2 peptide interferes with the NSF-dependent

disassembly of the SNARE complex (ref. 28).

3. A single point mutation of the NSF3 peptide, resembling the *Drosophila* comatose mutation, completely prevents the peptide from inhibiting either ATPase activity or synaptic transmission (ref. 30).

Supplementary Figure

Figure S1:

Postulated dynamics of SNARE proteins during exocytosis. SV in the reserve pool contains *cis*-SNARE complexes (6). (A) αSNAP and NSF bind to *cis*-SNARE complexes on SV and plasma membranes (latter not shown for clarity). (B) αSNAP and SNAREs stimulate the ATPase activity of NSF, causing disassembly of *cis*-SNARE complexes. NSF may remain bound on SV even after unbinding of αSNAP (7). (C) Free SNARE proteins form *trans*-SNARE complexes. (D) During or shortly after membrane fusion, when SV and plasma membranes are continuous, SNARE proteins are sorted onto the correct compartment. Acceptor proteins for respective SNARE proteins are not shown for clarity. (E) *Cis*-SNARE complexes are retrieved along with the SV membrane during endocytosis. (F) Recycling SVs contain *cis*-SNARE complexes (8).

Supplementary References

1. Mitchison, T. J., Sawin, K. E., Theriot, J. A., Gee, K. & Mallavarapu, A. (1998) *Methods Enzymol* 291, 63-78.

2. Gee, K. R., Weinberg, E. S. & Kozlowski, D. J. (2001) *Bioorg Med Chem Lett* 11, 2181-3.

3. Augustine, G. J. & Eckert, R. (1984) *J Physiol (Lond)* 346, 257-71.

4. Augustine, G. J., Charlton, M. P. & Smith, S. J. (1985) *J Physiol (Lond)* 367, 143-62.

5. Schmitt, B. M. & Koepsell, H. (2002) *Biophys J* 82, 1345-57.

6. Hong, R. M., Mori, H., Fukui, T., Moriyama, Y., Futai, M., Yamamoto, A., Tashiro, Y. & Tagaya, M. (1994) *FEBS Lett* 350, 253-7.

7. Mayer, A., Wickner, W. & Haas, A. (1996) *Cell* 85, 83-94.

8. Steel, G. J., Tagaya, M. & Woodman, P. G. (1996) *Embo J* 15, 745-52.

Kuner et al., Figure S1